

SOLVING HELMHOLTZ EQUATION BY MESHLESS RADIAL BASIS FUNCTIONS METHOD

S. J. Lai and B. Z. Wang

Institute of Applied Physics
University of Electronic Science and Technology of China
Chengdu 610054, China

Y. Duan

School of Applied Mathematics
University of Electronic Science and Technology of China
Chengdu 610054, China

Abstract—In this paper, we propose a brief and general process to compute the eigenvalue of arbitrary waveguides using meshless method based on radial basis functions (MLM-RBF) interpolation. The main idea is that RBF basis functions are used in a point matching method to solve the Helmholtz equation only in Cartesian system. Two kinds of boundary conditions of waveguide problems are also analyzed. To verify the efficiency and accuracy of the present method, three typical waveguide problems are analyzed. It is found that the results of various waveguides can be accurately determined by MLM-RBF.

1. INTRODUCTION

For the conducting waveguide problems, there are many diverse numerical procedures to solve the Helmholtz equation. These numerical procedures include traditional and advanced numerical methods, such as finite element method (FEM) [1], coupled transverse-mode integral Equation [2], moment method [3], finite difference frequency domain method [4], multipole expansion technique [5], and the methods of external excitation [6], of which the interpolation procedure is implemented on a certain regular mesh.

In recent years, meshfree or meshless methods based on a set of independent points have been used to solve the Helmholtz equation.

For example, hybrid boundary-node method [7], boundary knot method [8], radial point interpolation method (RPIM) [9], meshfree least square-based finite difference method [10], and Element-free Galerkin (EFG) method [11], have been applied to the Helmholtz equation. EFG was also applied to the time-domain field problem [12]. Some of these meshless methods were reported to have some advantages: Significantly lower dispersion than the FEM [9], high convergence rates and high accuracy [7], and suitable for complicate geometry simulation [8].

The scattered data interpolation with radial basis functions (RBFs) which was first proposed by Kansa [13] in 1990 are powerful tools in multi-variable approximation. It has been successfully used to solve various partial differential equations which include the Helmholtz equation of waveguide problems. Zhao proposed a novel conformal meshless method based on RBF coupled with coordinate transformation technique to analyze arbitrary waveguide problems [14]. Elliptical waveguides are computed by meshless collocation method with Wendland RBFs [15]. Waveguide problem in cylindrical system is also solved by using radial basis function (RBF) method [16]. For time-domain Maxwell equations, the RBF method is applied to waveguide eigenvalue problems [17] and transient electromagnetic problems [18].

The purpose of this paper is to propose a brief and general process of meshless method based on the RBF interpolation technique (MLMRBF) to solve the Helmholtz equation of arbitrary waveguide problems. The proposed MLM-RBF is a weighted residual method that is based on the RBF interpolation technique at a set of independent points and the weighted residual procedure adopts the point matching method. This paper is organized as follows. In Section 2, the RBF interpolation technique and the discretization formulation of Helmholtz equation by MLM-RBF will be described. In Section 3, we will use three typical waveguide problems to validate the proposed method. Section 4 is the conclusion.

2. RADIAL BASIS FUNCTION MESHLESS APPROACH FOR HELMHOLTZ EQUATION

2.1. The RBF Interpolation Method

The unknown function $U(\mathbf{r})$ in the computation domain Ω can be interpolated approximately by a series of RBF:

$$U(\mathbf{r}) \approx U^h(\mathbf{r}) = \sum_{I=1}^N a_I \phi_I(\mathbf{r}), \quad \mathbf{r} \in \Omega \quad (1)$$

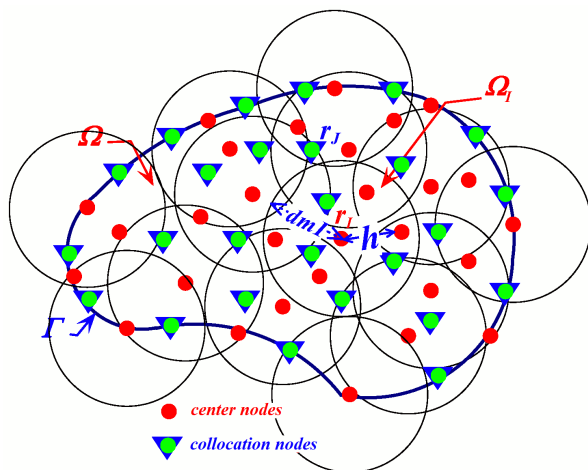


Figure 1. The distribution of center nodes \mathbf{r}_I and collocation nodes \mathbf{r}_J , supported domain radius d_{mI} and node distance h in the computation domain Ω .

where $\phi_I(\mathbf{r}) = \phi(\|\mathbf{r} - \mathbf{r}_I\|)$, is the radial basis function centered at a set of independent points $\mathbf{r}_1, \dots, \mathbf{r}_I, \dots, \mathbf{r}_N \in \Omega$ (also called center nodes, see Fig. 1), a_I are unknown coefficients to be computed and $\|\bullet\|$ represents the Euclidean distance r between the node \mathbf{r} and the center node \mathbf{r}_I .

It's known that node distribution affects the results of the RBF interpolation. In order to obtain the accurate interpolation, nodes in the computation domain Ω need nearly homogeneous distribution; nodes close to and at the boundaries need high density [19].

According to the range of RBFs' supported domain, RBFs can be classified into two types: The globally supported RBFs and the compactly supported RBFs. In this paper, two global RBFs and one compact RBF are chosen to solve the waveguide problems. They are the global Gaussian RBF with shape parameter c :

$$\phi_I(\mathbf{r}) = \exp(-c\|\mathbf{r} - \mathbf{r}_I\|^2), \tag{2}$$

the global quintic RBF without shape parameter:

$$\phi_I(\mathbf{r}) = \|\mathbf{r} - \mathbf{r}_I\|^5, \tag{3}$$

and the compact RBF given by Wu [20]:

$$\phi_I(\mathbf{r}) = (1 - r)_+^6 (6 + 36r + 82r^2 + 72r^3 + 30r^4 + 5r^5) \tag{4}$$

where

$$r = \frac{\|\mathbf{r} - \mathbf{r}_I\|}{d_{mI}} \tag{5}$$

in which d_{mI} is the radius of supported domain (also called supported parameter) of RBF at the center node \mathbf{r}_I and

$$(1-r)_+ = \begin{cases} 1-r, & 0 \leq r \leq 1 \\ 0, & \text{other} \end{cases} \quad (6)$$

From (1), we can see that the partial derivative of $u^h(\mathbf{r})$ is only related to RBF. The first-order partial derivatives of RBF can be expressed as

$$\partial_p \phi_I(\mathbf{r}) = \frac{\partial \phi_I(\mathbf{r})}{\partial r} \frac{\partial r}{\partial p} \quad (7)$$

where p represents x , y or z in Cartesian system and

$$\frac{\partial r}{\partial p} = \frac{p - p_I}{coe * \|\mathbf{r} - \mathbf{r}_I\|} \quad (8)$$

in which $coe = 1$ for global RBFs, while according to (5), $coe = d_{mI}$ for compact RBFs.

The second-order partial derivative of RBF can be expressed as:

$$\partial_{pq} \phi_I(\mathbf{r}) = \frac{\partial^2 \phi_I(\mathbf{r})}{\partial r^2} \frac{\partial r}{\partial p} \frac{\partial r}{\partial q} + \frac{\partial \phi_I(\mathbf{r})}{\partial r} \frac{\partial^2 r}{\partial p \partial q} \quad (9)$$

where q represents x , y or z in Cartesian system, and $\partial^2 \mathbf{r} / \partial p \partial q$ is obtained via (8)

$$\frac{\partial^2 \mathbf{r}}{\partial p \partial q} = \frac{1}{coe * \|\mathbf{r} - \mathbf{r}_I\|^3} \left[\frac{\partial p}{\partial q} \|\mathbf{r} - \mathbf{r}_I\|^2 - (p - p_I)(q - q_I) \right] \quad (10)$$

2.2. Helmholtz Equation Expressed by MLM-RBF

Suppose that the waveguide boundaries are parallel to the longitudinal z (see Fig. 2). The Borgnis' function $U(\mathbf{r})$ satisfies the homogenous scalar Helmholtz equation in two-dimensional (2D) Cartesian system [21]:

$$\frac{\partial^2 U(\mathbf{r})}{\partial x^2} + \frac{\partial^2 U(\mathbf{r})}{\partial y^2} + \lambda^2 U(\mathbf{r}) = 0, \quad \mathbf{r} \in \Omega \quad (11)$$

where $\lambda^2 = k^2 - k_z^2$, k represents the propagation constant, k_z represents the longitudinal propagation constant. For the transverse magnetic (TM) mode case, the boundary conditions of $U(\mathbf{r})$ on Γ satisfy

$$U(\mathbf{r})|_{\Gamma} = 0 \quad (12)$$

And the boundary conditions of transverse electric (TE) mode satisfy

$$\left. \frac{\partial U(\mathbf{r})}{\partial n} \right|_{\Gamma} = 0 \quad (13)$$

where ∂n represents the normal derivative on the boundary Γ .

Substituting the RBF interpolation function (1) into (11) and two boundary conditions (12), (13), we get the RBF interpolation formulation of Helmholtz equation

$$\begin{cases} \sum_{I=1}^N a_I [\partial_{xx}\phi_I(\mathbf{r}) + \partial_{yy}\phi_I(\mathbf{r}) + \lambda^2\phi_I(\mathbf{r})] = 0, & \mathbf{r} \text{ in } \Omega \\ \sum_{I=1}^N a_I\phi_I(\mathbf{r}) = 0, & \mathbf{r} \text{ on } \Gamma, \text{ for TM mode} \\ \sum_{I=1}^N a_I\partial_n\phi_I(\mathbf{r}) = 0, & \mathbf{r} \text{ on } \Gamma, \text{ for TE mode} \end{cases} \quad (14)$$

Then, point-matching method is applied to Equation (14) at a set of collocation nodes $\mathbf{r}_1, \dots, \mathbf{r}_J, \dots, \mathbf{r}_M \in \Omega$ ($M \geq N$) (see Fig. 1). Thus, we get the discretization formulations of Helmholtz equation of TM and TE modes by MLM-RBFs. They could be written by the matrix formulation:

$$\mathbf{A}\mathbf{a} = -\lambda^2\mathbf{B}\mathbf{a} \quad (15)$$

where the vector coefficient $\mathbf{a} = [a_1, \dots, a_N]^T$, the individual elements of matrix \mathbf{A} can be written as

$$A_{IJ} = \begin{cases} \partial_{xx}\phi_I(\mathbf{r}_J) + \partial_{yy}\phi_I(\mathbf{r}_J), & \mathbf{r}_J \text{ in } \Omega \\ \phi_I(\mathbf{r}_J), & \mathbf{r}_J \text{ on } \Gamma, \text{ for TM mode} \\ \partial_n\phi_I(\mathbf{r}_J), & \mathbf{r}_J \text{ on } \Gamma, \text{ for TE mode} \end{cases} \quad (16)$$

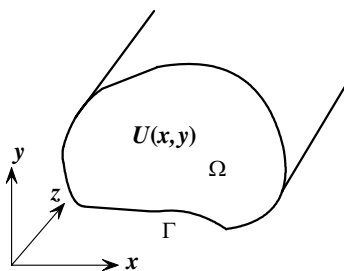


Figure 2. The structure of arbitrary waveguide.

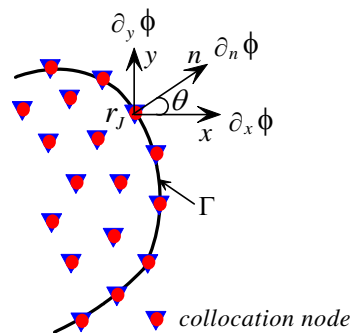


Figure 3. The $\partial_x\phi$ and $\partial_y\phi$ projected on the normal direction on \mathbf{r}_J of the arbitrary curved boundary.

in which the $\partial_n\phi$ equals to the sum of $\partial_x\phi$ and $\partial_y\phi$ projected on the normal direction (see Fig. 3):

$$\begin{aligned} \partial_n\phi_I(\mathbf{r}_J) &= \partial_x\phi_I(\mathbf{r}_J) \cdot \cos(\hat{n}, \hat{x}) + \partial_y\phi_I(\mathbf{r}_J) \cdot \cos(\hat{n}, \hat{y}) \\ &= \partial_x\phi_I(\mathbf{r}_J) \cdot \cos(\theta) + \partial_y\phi_I(\mathbf{r}_J) \cdot \sin(\theta) \end{aligned} \tag{17}$$

where \hat{x} , \hat{y} , and \hat{n} are unit vectors in the x -, y -directions, and the normal direction on the boundary Γ respectively. The angle θ is between \hat{x} and \hat{n} (see Fig. 3).

For both TE and TM cases, the individual elements of the matrix \mathbf{B} in (15) are

$$B_{IJ} = \begin{cases} \phi_I(\mathbf{r}_J), & \mathbf{r}_J \text{ in } \Omega \\ 0, & \mathbf{r}_J \text{ on } \Gamma \end{cases} \tag{18}$$

Equation (15) is the generalized eigenvalue equation. When $M > N$, (15) is M equations in N unknowns, i.e., an overdetermined linear equation; the least square method can be used to solve it. In this study, suppose the collocation nodes locate on the center nodes, i.e., $M = N$. The eigenpairs λ_j, \mathbf{a}_j , can be computed from (14), and then substituting \mathbf{a}_j into (1), the field distribution of the j th-eigenmode can be obtained.

3. VALIDATION OF THE PROPOSED METHOD

In order to validate the proposed method, three typical waveguide problems are solved in this section: Rectangular waveguide, elliptic waveguide, and triangular waveguide. The eigenvalues of TM and TE

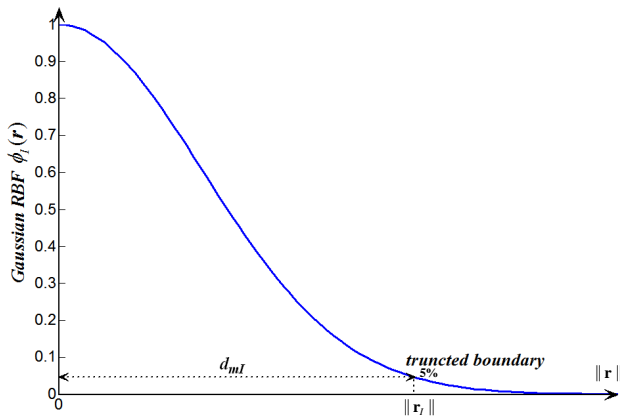


Figure 4. Truncated boundary of Gaussian RBF.

modes in each waveguide problem are calculated by MLM-RBFs with the global Gaussian, r^5 RBFs, and compact Wu's RBF. To analyze the accuracy of the numerical algorithm, the relative error is defined as follows:

$$Err = \frac{|\lambda_c - \lambda_{c0}|}{\lambda_{c0}} \times 100\% \tag{19}$$

where λ_c is the numerical cutoff wavelength by MLM-RBFs and λ_{c0} is the analytic solution. The results of MLM-RBFs are compared with those of the traditional mesh-based FDM and FEM methods on the condition that the node distribution is the same.

For a set of center nodes in the domain Ω , a node parameter h at \mathbf{r}_I , is defined as the minimum distance between the other nodes and \mathbf{r}_I , as shown in Fig. 1. In the global Gaussian RBF case, the shape parameter c influences the pulse width of supported domain. In the compact RBF case, d_{mI} influences the supported domain. So, for convenient analysis, the parameter c of Gaussian RBF needs to be transferred to d_{mI} . Suppose that the truncated boundary is set where the Gaussian RBF degenerates to 5% of its peak value and so the distance $\|\mathbf{r}_I\|$ is set as d_{mI} , as shown in Fig. 4. From (6), we can get

$$c = -\frac{\log(0.05)}{d_{mI}^2} \tag{20}$$

Usually, let d_{mI} be more than one time of h , so that the supported domain of RBFs at the nodes could be overlaid.

3.1. Standard BJ-100 Rectangular Waveguide

The structure of the standard waveguide BJ-100 (22.86 mm × 10.16 mm) is shown in Fig. 5. Suppose that the nodes distribute

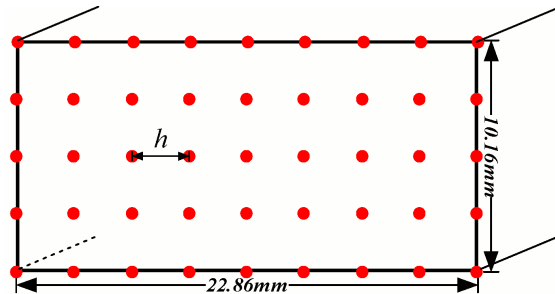


Figure 5. The node distribution of the standard BJ-100 waveguide.

Table 1. The cutoff wavelengths (λ_c/mm) and relative errors of TM mode by FDM, FEM and MLM-RBF in rectangular waveguide case.

mode	λ_{c0}	FDM	Err%	FEM	Err%	r^5 RBF	Err%	Gaussian RBF	Err%	Wu's RBF	Err%
TM ₁₁	1.8569	1.8608	0.21	1.8501	0.37	1.8570	0.01	1.8530	0.21	1.8549	0.11
TM ₂₁	1.5187	1.5220	0.22	1.5092	0.63	1.5185	0.01	1.5162	0.16	1.5174	0.09
TM ₃₁	1.2192	1.2235	0.35	1.2077	0.94	1.2187	0.04	1.2176	0.13	1.2183	0.07
TM ₄₁	0.9962	1.0023	0.61	0.9833	1.29	0.9958	0.04	0.9951	0.11	0.9957	0.05
TM ₁₂	0.9918	1.0011	0.94	0.9808	1.11	0.9929	0.11	0.9902	0.16	0.9915	0.03
TM ₂₂	0.9284	0.9363	0.85	0.9150	1.44	0.9289	0.05	0.9270	0.15	0.9280	0.04
TM ₃₂	0.8454	0.8522	0.80	0.8291	1.93	0.8452	0.02	0.8442	0.14	0.8449	0.06
TM ₅₁	0.8339	0.8422	0.99	0.8159	2.16	0.8337	0.02	0.8331	0.10	0.8336	0.04
TM ₄₂	0.7594	0.7660	0.87	0.7406	2.48	0.7587	0.09	0.7584	0.13	0.7589	0.07
TM ₆₁	0.7135	0.7241	1.49	0.6979	2.19	0.7135	0.00	0.7130	0.07	0.7135	0.00

noted: for the global Gaussian RBF case, $d_{mI} = 4.85 \times h$; for the compact Wus RBF case, $d_{mI} = 14.5 \times h$.

uniformly in \hat{x} - and \hat{y} -directions. The number of arranged nodes in rectangular region is set as 31×14 . In order to compare the calculation accuracy of the numerical methods, let the node distribution of FEM and FDM be the same as that of MLM-RBF.

The cutoff wavelengths and the relative errors of the ten lowest-order TM modes computed by MLM-RBF, FDM and FEM are shown in Table 1. From the Table, we can see that relative errors by MLM-RBF for all of the three RBFs are less than those by FDM and FEM. Furthermore, the relative errors by MLM-RBF are even an order of magnitude less than those by FDM and FEM for the higher-order modes after TM₄₁.

Figure 6 shows the comparison of the curves of relative errors by FDM, FEM, and MLM-RBF in the 60 lowest-order TM modes. From the figure, we can see that the relative errors of three numerical algorithms fluctuate slightly and increase generally as the order of mode increases. In the r^5 RBF and Wu's RBF cases, their relative errors are far less than those of FDM and FEM. The relative errors of Gaussian RBF case are still less than those of FDM and FEM although they change greatly when the order number is over 20.

Table 2 shows the results of ten lowest-orders TE modes computed by MLM-RBF, FDM and FEM. We can see that the relative errors for three RBFs' cases are a little less than those of FDM and FEM for

Table 2. The cutoff wavelengths (λ_c/mm) and relative errors of TE mode by FDM, FEM and MLM-RBF in rectangular waveguide case.

mode	λ_{c0}	FDM	Err%	FEM	Err%	r^5 RBF	Err%	Gaussian RBF	Err%	Wu's RBF	Err%
TE ₁₀	4.5720	4.5741	0.05	4.5699	0.05	4.5780	0.13	4.8074	5.15	4.6345	1.37
TE ₂₀	2.2860	2.2902	0.18	2.2819	0.18	2.2918	0.25	2.3205	1.51	2.2915	0.24
TE ₀₁	2.0320	2.0370	0.25	2.0271	0.24	2.0385	0.32	2.0507	0.92	2.0294	0.13
TE ₁₁	1.8569	1.8608	0.21	1.8501	0.37	1.8549	0.11	1.8743	0.94	1.8565	0.02
TE ₃₀	1.5240	1.5303	0.41	1.5180	0.39	1.5290	0.33	1.5323	0.54	1.5232	0.05
TE ₂₁	1.5187	1.5220	0.22	1.5090	0.64	1.5097	0.59	1.5268	0.53	1.5142	0.30
TE ₃₁	1.2192	1.2235	0.35	1.2078	0.94	1.2106	0.71	1.2224	0.26	1.2135	0.47
TE ₄₀	1.1430	1.1514	0.73	1.1347	0.73	1.1485	0.48	1.1455	0.22	1.1418	0.11
TE ₀₂	1.0160	1.0260	0.98	1.0062	0.96	1.0235	0.74	1.0135	0.25	1.0143	0.17
TE ₄₁	0.9962	1.0023	0.61	0.9836	1.26	0.9921	0.41	0.9973	0.11	0.9909	0.53

noted: for the global Gaussian RBF case, $d_{mI} = 5.79 \times h$; for the compact Wus RBF case, $d_{mI} = 20 \times h$.

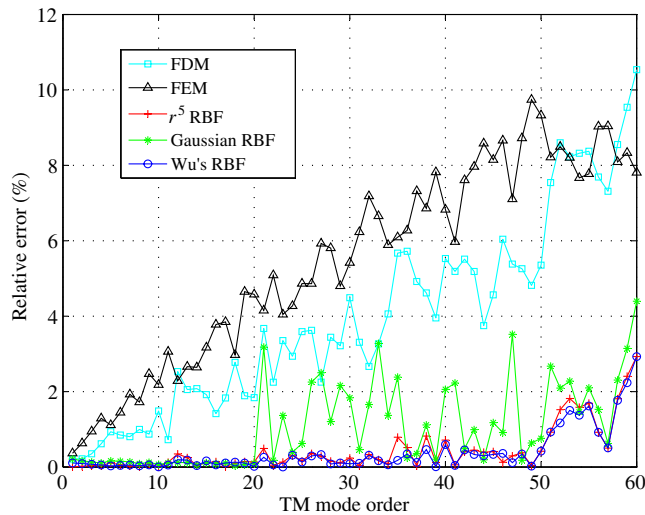


Figure 6. The relative errors of FDM, FEM and RBF-MLM vary with mode order increases in TM mode case.

most of TE modes. The case of r^5 -RBF without shape parameter is taken as a comparative example, the calculation accuracies of the TE modes are less than those of TM modes. In addition, like TM case, the relative errors by MLM-RBF do not always increase as the order of mode increases.

3.2. Elliptical Waveguide

In this section, the elliptical waveguide with curved boundary (see Fig. 7) is solved. Let long axis $b = 1$ and the eccentricity $e = 0.5$. The conformal node distribution fitting naturally the curved boundaries is adopted, as shown in Fig. 7. Let the number of node layer from center point to outer boundary be 10, and node distance on each layer be equal to layer distance h . Suppose the node distribution is the same as that of the FEM.

There are four types of propagation mode: TM_{cm} , TM_{sm} , TE_{cm} and TE_{sm} in elliptical waveguide, which are the hybrid modes of the linear combination of TM and TE modes in elliptical waveguide [22]. The subscripting symbol c , s represent odd mode and even mode in the hybrid modes respectively. The solution of ten lowest-order hybrid modes are computed by the modified continued fractional method [22]. In this paper, these hybrid modes are calculated directly by the TM and TE discretization formulation of MLM-RBF in Cartesian system.

Table 3 shows the results of ten lowest-orders hybrid modes computed by MLM-RBF and FEM. From the table, we can see that the relative errors of MLM-RBF are less than those of FEM for most of hybrid modes, especially for $TM_{c,s}$ mode cases whose accuracy is far

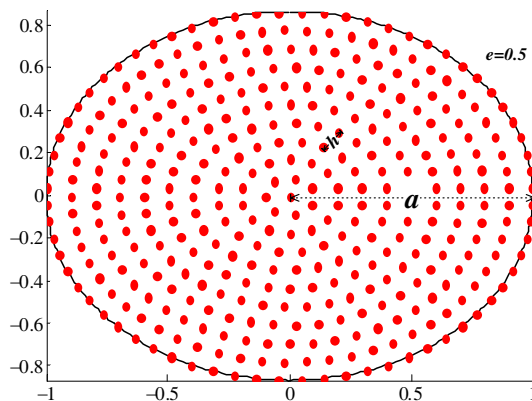


Figure 7. Nodes distribution of the elliptical waveguide.

Table 3. The cutoff wavelengths (λ_c/m) and relative errors of hybrid mode by FEM and MLM-RBF in elliptical waveguide case.

mode	λ_{c0}	FEM	Err%	r^5 RBF	Err%	Gaussian RBF	Err%	Wu's RBF	Err%
TE _{c11}	3.3945	3.3891	0.16	3.4147	0.60	3.4164	0.65	3.4308	1.07
TE _{s11}	2.9745	2.9688	0.20	2.9913	0.57	2.9809	0.22	2.9850	0.35
TM _{c01}	2.4196	2.4153	0.18	2.4184	0.05	2.4194	0.01	2.4188	0.03
TE _{c21}	1.9497	1.9430	0.34	1.9542	0.23	1.9514	0.09	1.9454	0.22
TE _{s21}	1.9079	1.9012	0.35	1.9092	0.07	1.9090	0.06	1.9031	0.25
TM _{c11}	1.5761	1.5675	0.55	1.5764	0.02	1.5760	0.01	1.5760	0.01
TE _{c01}	1.4994	1.4904	0.60	1.5121	0.85	1.4988	0.04	1.4927	0.45
TM _{s11}	1.4673	1.4577	0.65	1.4676	0.02	1.4672	0.01	1.4673	0.00
TE _{c31}	1.4027	1.3941	0.61	1.3947	0.57	1.4024	0.02	1.3940	0.62
TE _{s31}	1.3979	1.3896	0.59	1.3893	0.62	1.3975	0.03	1.3888	0.65

noted: for the global Gaussian RBF case, $d_{mI} = 7 \times h$; for the compact Wus RBF case, $d_{mI} = 20 \times h$.

greater than that of FEM. And the relative errors of TM_{c,s} modes are far less than those of TE_{c,s} modes. In three RBFs cases, the Gaussian RBF case has the maximum calculation accuracy, the relative errors of eight higher modes are less than 0.1% for TM_{c,s} or TE_{c,s} modes. Therefore, Gaussian RBF with a appropriate control parameter d_{mI} is a better choice to solve the elliptical waveguide using MLM-RBF.

Here, we just take TE_{c31} and TE_{s31} for example to show the field distribution by RBF-MLM with the global r^5 -RBF, as shown in Fig. 8. It can be seen that the field distribution perfectly represents the physical modes. Although the field distribution of both modes is similar, there is some little difference.

3.3. Right-angle Triangle Waveguide

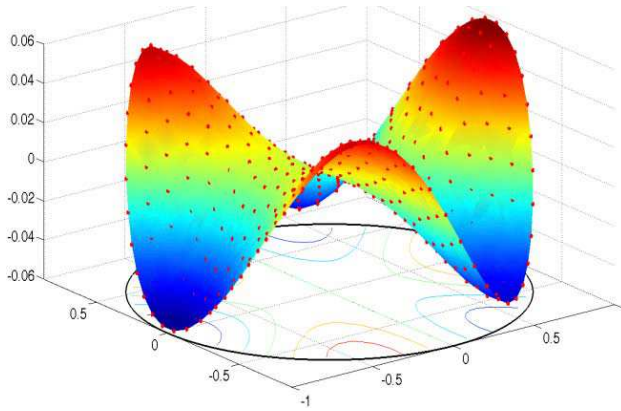
In this section, triangle waveguide with two sharp-angled boundaries is calculated by MLM-RBF. The structure and node distribution of right-angle triangle waveguide is shown in Fig. 9. Let the height of triangle waveguide $h_t = 1$ and the node number in each direction be 25. Suppose the node distribution is the same as that of FEM. In this example, only one global r^5 -RBF is chosen to compute the eight lowest-order TM and TE modes of triangle waveguide.

The analytic cutoff wavelength of TM and TE modes in triangle

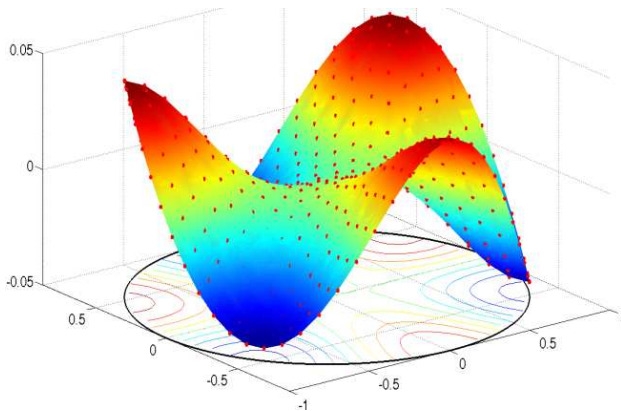
waveguide is given by [23] as follows

$$\begin{cases} \lambda_{c0TM} = \frac{\pi}{\sqrt{2}h_t} \sqrt{m^2 + (m + 2n - 1)^2} \\ \lambda_{c0TE} = \frac{m\pi}{h_t}, \frac{n\pi}{\sqrt{2}h_t} \end{cases}, \quad m, n = 1, 2, \dots \quad (21)$$

(**r_J**) Table 4 shows the results of the TM modes by MLM-RBF and FEM. From the table, we can see that the relative errors of MLM-RBF are an order of magnitude less than those of FEM except for TM₄₁ mode. Due to no control parameter of r^5 -RBF, the condition numbers



(a) TE_{c31}



(b) TE_{s31}

Figure 8. Field distribution of two hybrid modes by MLM-RBF with global r^5 RBF in elliptical waveguide.

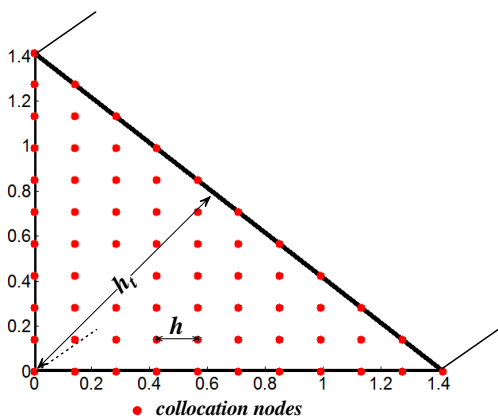


Figure 9. Node distribution of the right-angle triangle waveguide.

Table 4. The cutoff wavelengths (λ_c/m) and relative errors of TM mode by FEM and MLM-RBF in triangle waveguide case.

	TM ₁₁		TM ₂₁	TM ₁₂		TM ₃₁		TM ₂₂		TM ₁₃	TM ₄₁		TM ₃₂
λ_{c0}	1.2649		0.7845	0.6860		0.5657		0.5252		0.4650	0.4417		0.4216
FEM	1.2606	0.8875	0.7774	0.6776	0.6218	0.5561	0.5447	0.5132	0.4708	0.4533	0.4337	0.4301	0.4059
Err %	0.34		0.91	1.22		1.70		2.28		2.52	1.81		3.72
r^5 -RBF	1.2649	0.8946	0.7844	0.6864	0.6326	0.5655	0.5553	0.5255	0.4851	0.4658	0.4477	0.4415	0.4218
Err %	0.00		0.01	0.06		0.04		0.06		0.17	1.36		0.05

Table 5. The cutoff wavelengths (λ_c/m) and relative errors of TE mode by FEM and MLM-RBF in triangle waveguide case.

	TE ₁	TE ₂	TE ₃		TE ₄	TE ₅			TE ₆		TE ₇		TE ₈
λ_{c0}	2.8284	2.0	1.4142		1.0	0.9428			0.7071		0.6667		0.5657
FEM	2.8266	1.9961	1.4105	1.2583	0.9923	0.9373	0.8875	0.7727	0.6998	0.6775	0.6556	0.6213	0.5566
Err %	0.06	0.20	0.26		0.77	0.58			1.03		1.66		1.61
r^5 -RBF	2.8267	1.9941	1.4127	1.2583	0.9945	0.9433	0.8889	0.7788	0.7065	0.6827	0.6621	0.6265	0.5662
Err %	0.06	0.30	0.11		0.55	0.05			0.09		0.69		0.09

of coefficient matrix **A** and **B** in (15) are great up to 10^{10} . In addition, according to analytical formula (21), there exist many redundant solutions for both MLM-RBF and FEM. The field distributions of TM₂₁ and TM₃₂ modes by RBF-LMLM with the global r^5 -RBF are shown in Fig. 10. It can be seen that the field distribution perfectly represents the physical modes.

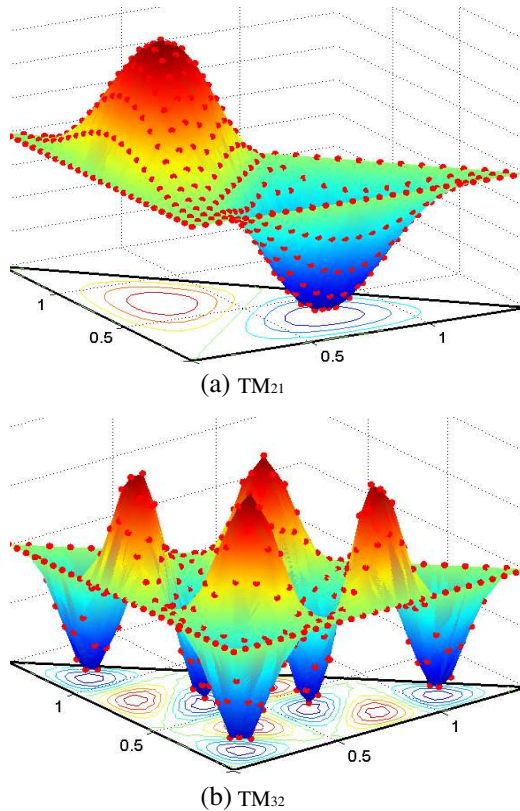


Figure 10. Field distribution of two TM modes by MLM-RBF with global r^5 -RBF in triangular waveguide.

The results of the eight lowest-order TE modes of the triangle waveguide by MLM-RBF and FEM are shown in Table 5. Like TM case, we can see that the relative errors of MLM-RBF are less than those of FEM and there exist redundant solutions. In addition, in this waveguide case, the relative errors of MLM-RBF are far less than those of FEM for all TE modes, which is obviously different from the former two waveguide cases in which the relative errors of MLM-RBF are close to those of FEM and FDM. It is because node density of triangle waveguide is far more than the former two that the high convergence rate and high accuracy could be obtained [7].

About the algorithm complexity of the present method, from (16) and (7)–(10), we can see that each element of matrix \mathbf{A} require about twenty multiplications for r^5 RBF case (more than 20 for the other RBFs). In addition, the non-zero elements for each matrix column

equal to the number of collocation node in the supported domain of the center node. Usually, the supported domain of RBF expands more than one node, even above ten nodes. Thus, the present algorithm complexity is much more than FEM and FDM.

4. CONCLUSION

In this paper, MLM-RBF has been applied to solve the scalar Helmholtz equation in Cartesian system. The global Gaussian, r^5 and compact Wu's RBFs are used to compute the cutoff wavelength of three specific waveguide problems. To analyze the accuracy of proposed method, the node distribution of meshless method is set the same as the those of mesh-based FDM and FEM.

In rectangular waveguide case, by comparing the results of MLM-RBF with those of FDM and FEM, higher accuracy can be seen in both TM and TE modes by the proposed method with all three RBF cases. The calculation errors of MLM-RBF increase generally as the order of mode increases like FDM and FEM.

In elliptical waveguide case, under the natural conformal node distribution, the results of RBF-MLM for three RBFs cases have very higher calculation accuracy than those of FEM. The Gaussian RBF case has the highest calculation accuracy in three RBFs cases.

In right-angle triangle waveguide case, the results of MLM-RBF with r^5 -RBF are in agreement with the analytic solutions. For most of the modes, the relative errors of MLM-RBF are far less than those of FEM. However, there are some pseudo solutions in both MLM-RBF and FEM.

In three typical waveguide problems, the field distributions of TE and TM modes perfectly represents the physical mode distribution, which shows that the field distributions could be correctly calculated by the proposed method. The calculation accuracy of MLM-RBF is greater than that of mesh-based FDM and FEM, especially for the Dirichlet problem of waveguides. However, the calculation amount of MLM-RBF is more than that of FEM and FDM. The present process of MLM-RBF is a brief and general meshless method, which can be flexibly applied to compute the eigenvalues of arbitrary waveguides.

ACKNOWLEDGMENT

This work was supported by the High-Tech Research and Development Program of China (No. 2008AA01Z206) and the National Natural Science Foundation of China (No. 10926190, No. 60872029 and No. 60872034), and Project 9140A01020110DZ0211.

REFERENCES

1. Arlett, P. L., A. K. Bahrani, and O. C. Zienkiewicz, "Application of finite element to the solution of Helmholtz's equation," *Proc. IEE.*, Vol. 115, No. 12, 1762–1766, 1968.
2. Chang, H. W., Y. H. Wu, S. M. Lu, W. C. Cheng, and M. H. Sheng, "Field analysis of dielectric waveguide devices based on coupled transverse-mode integral equation — Numerical investigation," *Progress In Electromagnetics Research*, Vol. 97, 159–176, 2009.
3. Khalaj-Amirhosseini, M., "Analysis of longitudinally inhomogeneous waveguides using the method of moments," *Progress In Electromagnetics Research*, Vol. 74, 57–67, 2007.
4. Lavranos, C. S. and G. A. Kyriacou, "Eigenvalue analysis of curved open waveguides using a finite difference frequency domain method employing orthogonal curvilinear coordinates," *PIERS Online*, Vol. 1, No. 3, 271–275, 2005.
5. Seydou, F., T. Seppanen, and O. M. Ramahi, "Computation of the Helmholtz eigenvalues in a class of chaotic cavities using the multipole expansion technique," *IEEE Transactions on Antennas and Propagation*, Vol. 57, No. 4, 1169–1177, 2009.
6. Reutskiy, S. Y., "The methods of external excitation for analysis of arbitrarily-shaped hollow conducting waveguides," *Progress In Electromagnetics Research*, Vol. 82, 203–226, 2008.
7. Miao, Y., Y. Wang, and Y. H. Wang, "A meshless hybrid boundary-node method for Helmholtz problems," *Eng. Anal. Boundary Elem.*, Vol. 33, No. 2, 120–127, 2009.
8. Hon, Y. C. and W. Chen, "Boundary knot method for 2D and 3D Helmholtz and convection-diffusion problems under complicated geometry," *Int. J. Numer. Methods Eng.*, Vol. 56, No. 13, 1931–1948, 2003.
9. Christina, W. and O. Von Estorff, "Dispersion analysis of the meshfree radial point interpolation method for the Helmholtz equation," *Int. J. Numer. Methods Eng.*, Vol. 77, No. 12, 1670–1689, 2009.
10. Shu, C., W. X. Wu, and C. M. Wang, "Analysis of metallic waveguides by using least square-based finite difference method," *Comput. Mater. Continua.*, Vol. 2, No. 3, 189–200, 2005.
11. Ooi, B. L. and G. Zhao, "Element-free method for the analysis of partially-filled dielectric waveguides," *Journal of Electromagnetic Waves and Applications*, Vol. 21, No. 2, 189–198, 2007.
12. Liu, X. F., B. Z. Wang, and S. J. Lai, "Element-free Galerkin

- method for transient electromagnetic field simulation,” *Microw. Opt. Techn. Lett.*, Vol. 50, No. 1, 134–138, 2008.
13. Kansa, E. J., “Multiquadrics — A scattered data approximation scheme with applications to computational fluid-dynamics — I: Surface approximations and partial derivatives,” *Computer Math. Applic.*, Vol. 9, No. 8–9, 127–145, 1992.
 14. Zhao, G., B. L. Ooi, Y. J. Fan, Y. Q. Zhang, I. Ang, and Y. Gao, “Application of conformal meshless RBF coupled with coordinate transformation for arbitrary waveguide analysis,” *Journal of Electromagnetic Waves and Applications*, Vol. 21, No. 1, 3–14, 2007.
 15. Jiang, P. L., S. Q. Li, and C. H. Chuan, “Analysis of elliptical waveguides by a meshless collocation method with the Wendland radial basis functions,” *Microwave Opt. Technol. Lett.*, Vol. 32, No. 2, 162–165, 2002.
 16. Yu, J. H. and H. Q. Zhang, “Solving waveguide eigenvalue problem by using radial basis function method,” *World Autom. Congr., WAC*, Vol. 1, 1–5, 2008.
 17. Lai, S. J., B. Z. Wang, and Y. Duan, “Application of the RBF-based meshless method to solve 2-D time domain maxwells equations,” *Int. Conf. Microw. Millimeter Wave Technol. Proc., ICMMT*, Vol. 2, 749–751, 2008.
 18. Lai, S. J., B. Z. Wang, and Y. Duan, “Meshless radial basis function method for transient electromagnetic computations,” *IEEE Trans. Magn.*, Vol. 44, No. 10, 2288–2295, 2008.
 19. Fornberg, B., T. A. Driscoll, G. Wright, and R. Charles, “Observations on the behavior of radial basis function approximation near boundaries,” *Comput. Math. Appl.*, Vol. 43, No. 3, 473–490, 2002.
 20. Wu, Z. M., “Compactly supported positive definite radial functions,” *Adv. Comput. Math.*, Vol. 4, 283–292, 1995.
 21. Zhang, K. Q. and D. J. Li, *Electromagnetic Theory for Microwaves and Optoelectronics*, Chapter 4, Springer Press, New York, 2008.
 22. Zhang, S. J. and Y. C. Shen, “Eigenmode sequence for an elliptical waveguide with arbitrary ellipticity,” *IEEE Trans. MTT.*, Vol. 43, No. 1, 221–224, 1995.
 23. Lin, W. G., *Microwave Theory and Techniques*, 158–162, Science Press, Beijing, 1979 (in Chinese).